

Comparative study of superdeformed and highly deformed bands in the $A \sim 60$ mass region

A. V. Afanasjev,^{1,2,3} I. Ragnarsson,³ and P. Ring¹

¹Physik-Department der Technischen Universität München, D-85747 Garching, Germany

²Nuclear Research Center, Latvian Academy of Sciences, LV-2169, Salaspils, Miera str. 31, Latvia

³Department of Mathematical Physics, Lund Institute of Technology, P.O. Box 118, S-22100, Lund, Sweden

(Received 17 February 1999)

Superdeformed and highly deformed rotational bands in the $A \sim 60$ mass region are studied within cranked relativistic mean field theory and the configuration-dependent cranked Nilsson-Strutinsky approach. Both approaches describe the experimental data well. Low values of the dynamic moments of inertia $J^{(2)}$ compared with the kinematic moments of inertia $J^{(1)}$ seen both in experiment and in calculations at high rotational frequencies indicate the high energy cost to build the states at high spin and reflect the limited angular momentum content in these configurations. [S0556-2813(99)05906-3]

PACS number(s): 27.40.+z, 27.50.+e, 21.10.Re, 21.60.Jz

I. INTRODUCTION

Extremely fast rotating nuclei are interesting laboratories providing information for test of theoretical models at extreme conditions (large angular momentum and/or deformation, limit of angular momentum in the rotational bands, etc.). At high rotational frequencies pairing correlations are considerably quenched and can often be neglected. A most interesting nuclear region is the one with $A \sim 60$ ($N \approx Z \approx 30$), where a large variety of rotational structures such as (smooth) terminating, highly deformed, and superdeformed (SD) rotational bands are expected to be observed up to very high rotational frequencies in the same nucleus. The ^{62}Zn nucleus [1,2] represents a first example of this variety.

Of special interest are the SD bands in this region since they extend to the highest rotational frequencies (~ 1.8 MeV) observed so far in SD bands. The fact that the predicted SD band in the doubly magic superdeformed nucleus ^{60}Zn [3] has been observed [4] and that it is linked to the low-spin level scheme is another attractive point. This is because by means of an effective alignment (or similar) approach [5,6], it becomes possible to map not only relative spin values as in the $A \sim 140$ – 150 mass region (see Refs. [6,7]), but also absolute spin values in the unlinked SD and highly deformed bands. Then, in SD bands with little influence of pairing correlations, it will be possible to make a comparison between experiment and theory, not only for those physical observables which can be extracted without knowing absolute spin values (like dynamic moment of inertia $J^{(2)}$ and the transition quadrupole moment Q_2), but also, for the first time, for observables which cannot be extracted without such knowledge (like the kinematic moment of inertia $J^{(1)}$ and the evolution of the excitation energy within a band as a function of spin).

In the present article, a comparative study of the recently observed highly deformed band in ^{58}Cu [8] and the SD bands in $^{60,62}\text{Zn}$ [1,4] is presented. In addition, the general features of SD and highly deformed bands in this mass region of $A \sim 60$ are outlined.

II. THEORETICAL TOOLS AND DETAILS OF CALCULATIONS

Our theoretical tools are cranked relativistic mean field (CRMF) theory [9,10] and the configuration-dependent cranked Nilsson-Strutinsky (CNS) approach [11,12]. In relativistic mean field (RMF) theory the nucleus is described as a system of pointlike nucleons represented by Dirac spinors and coupled to mesons and to the photon. The nucleons interact by the exchange of several mesons, namely, the scalar σ and three vector particles: ω , ρ , and the photon. CRMF theory represents the extension of RMF theory to the rotating frame. CRMF theory is a fully self-consistent theory. On the contrary, in the CNS approach the total energy is described as a sum of the rotating liquid drop energy and the shell correction energy. This leaves some room for inconsistencies between macroscopic and microscopic parts as illustrated, for example, in Refs. [13,14]. However, it is commonly accepted that the CNS approach provides a reasonable description of the nuclear many-body problem. Both models have been very successful in describing different aspects of SD bands in the $A \sim 140$ – 150 mass region (see, e.g., [7,15] and [6,13]). The details of the formalisms of these two approaches can be found in Refs. [7,15] and in Refs. [11,12], respectively.

CRMF calculations have been performed with three parametrizations of the RMF Lagrangian (NL1 [16], NL3 [17], and NLSH [18]) in order to define the force best suited for the description of rotational properties of the nuclei with $N \approx Z$. Since the results with NL3 are rather close to the ones with NLSH, they are not shown in all figures. The spatial components of the vector mesons (*nuclear magnetism*) play an extremely important role for the description of moments of inertia [19]. They are taken into account in a fully self-consistent way.

The cranked relativistic mean field equations are solved in the basis of a deformed harmonic oscillator. A basis deformation of $\beta_0 = 0.2$ has been used. All bosonic states below the energy cutoff $E_B^{\text{cut-off}} \leq 16.5\hbar\omega_0^B$ and all fermionic states below the energy cut-off $E_F^{\text{cut-off}} \leq 13.5\hbar\omega_0^F$ have been used in the diagonalization. The increase of the fermionic space

compared with the truncation scheme used in Ref. [7] was necessary because in the present study, we compare experimental and calculated excitation energies relative to a rigid rotor reference which requires high accuracy in the calculation of energies. Note, however, that the energy cut-off $E_F^{\text{cut-off}} \leq 11.5\hbar\omega_0^F$ provides a rather good description of moments of inertia and the quadrupole and hexadecapole moments, and thus it can be used for a more systematic investigation.

In the CNS calculations, the Nilsson potential with the standard set of parameters [11] has been used. In both approaches, pairing correlations are not taken into account. Therefore, the results can be considered as realistic only in the region of high spins, say, $I \geq 15\hbar$. However, for some configurations the paired band crossings at low spin will be blocked and thus, in these cases, the results of the calculations are not expected to deviate significantly from experiment even at lower spin values; for details see the discussion in Ref. [15]. To label the configurations we use the shorthand notation $[p_1p_2, n_1n_2]$ where $p_1(n_1)$ is the number of proton (neutron) $f_{7/2}$ holes and $p_2(n_2)$ is the number of proton (neutron) $g_{9/2}$ particles. Superscripts to the configuration labels (e.g., $[22,22]^+$) and orbital labels (e.g., $[413]3/2^+$) are used to indicate the sign of the signature r for that configuration ($r = \pm 1$) or that orbital ($r = \pm i$).

III. RESULTS AND DISCUSSION

According to the CRMF and the CNS approaches, the doubly magic SD band in ^{60}Zn has a $[22,22]^+$ structure in the notation defined above. In this configuration, all single-particle levels below the $Z=N=30$ SD shell gaps are occupied (see Fig. 1). At the spins of interest, this band is well separated from excited SD configurations (see Fig. 3 in Ref. [4]). The experimental observables ($J^{(1)}, J^{(2)}$ at $\Omega_x \geq 1.1$ MeV and Q_i) are well described in both approaches [see Figs. 2(c), 2(d), and 4, below]. At $\Omega_x \sim 0.95$ MeV, the observed band undergoes a paired band crossing, the description of which is not addressed in the present calculations. Note that this is a $N=Z$ nucleus; so the proton-neutron pairing correlations could play some role at high spin.

Contrary to ^{60}Zn , the bands in ^{58}Cu and ^{62}Zn are not linked to the low-spin level scheme and thus their parities and spins are not known experimentally. One way to establish these quantities is to use an effective alignment approach [5]. The effective alignment between bands A and B is defined (see Ref. [5]) as $i_{\text{eff}}^{A,B}(\Omega_x) = I_B(\Omega_x) - I_A(\Omega_x)$. Band A in the lighter nucleus is taken as a reference: so the effective alignment measures the effect of additional particles. The practical application of this approach is illustrated in Fig. 3(a) where the calculated i_{eff} 's between the $[21,21]^-$ configuration in ^{58}Cu and the $[22,24]^+$ configuration in ^{62}Zn are compared with experimental i_{eff} 's in the $^{58}\text{Cu}/^{62}\text{Zn}$ pair. The ‘‘experimental’’ i_{eff} are drawn using the spin values given in the caption to Fig. 3, where the fixed spin value of $I_0 = 9$ for the lowest observed state in the ^{58}Cu band is consistent with the results of the analysis below. The values of I_0 should be chosen according to the signature r of the assigned configuration, e.g., even values of I_0 for $r = 1$. It is clear that it is only for the value of $I_0 = 18$ for the lowest state in the ^{62}Zn band that a good agreement is obtained between ‘‘exper-

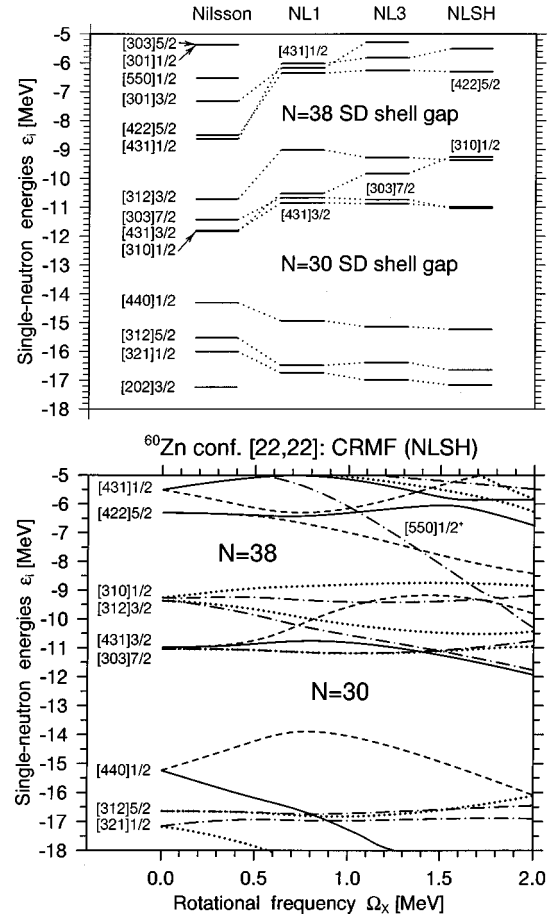


FIG. 1. Bottom panel: neutron single-particle energies (Routhians) in the self-consistent rotating potential as a function of the rotational frequency Ω_x calculated in CRMF theory with parameter set NLSH. They are given along the deformation path of the lowest SD configuration $[22,22]^+$ in ^{60}Zn . Solid, short-dashed, dot-dashed, and dotted lines indicate $(\pi = +, r = -i)$, $(\pi = +, r = +i)$, $(\pi = -, r = +i)$, and $(\pi = -, r = -i)$ orbitals, respectively. At $\Omega_x = 0.0$ MeV, the single-particle orbitals are labeled by the asymptotic quantum numbers $[Nn_z\Lambda]\Omega$ (Nilsson quantum numbers) of the dominant component of the wave function. Top panel: the single-particle states around the $N=30$ SD shell gap calculated with the Nilsson potential and three parametrizations of RMF theory at the corresponding equilibrium deformations of the $[22,22]^+$ configuration in ^{60}Zn at $\Omega_x = 0.0$ MeV. It is only in the CRMF calculations that the energies are absolute, in the Nilsson potential the energies are shifted so that the $N=30$ SD shell gaps coincide roughly in both approaches. The relative single-particle energies are approximately the same for the protons as for the neutrons, but the absolute proton energies are higher because of the Coulomb energy. The fact that the spectrum is less dense in RMF theory than in the Nilsson potential is related to low effective mass ($m^*/m \approx 0.6$) in RMF theory.

mental’’ and calculated values of i_{eff} .

Note that $i_{\text{eff}}[A(I_0^A)/B(I_0^B)] = i_{\text{eff}}[A(I_0^A + n)/B(I_0^B + n)]$ (n is an integer); i.e., the effective alignment approach can be used to determine relative spin values. Therefore, this approach is particularly relevant in the present case where the absolute spin values are known for the SD band in ^{60}Zn . It should thus be possible to obtain absolute spin values for the unlinked highly deformed band in ^{58}Cu and the SD band in

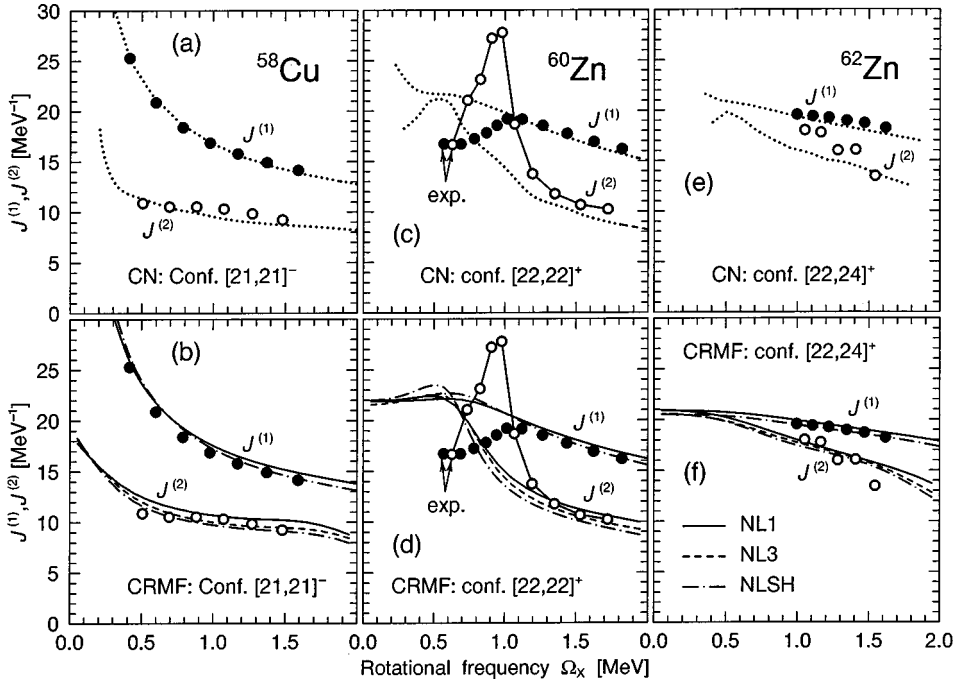


FIG. 2. Kinematic $J^{(1)}$ (unlinked solid circles) and dynamic $J^{(2)}$ (open circles) moments of inertia of observed bands versus the ones of assigned calculated configurations. The notation of lines is given in the figure. The values of $J^{(1)}$ calculated with NL3 are typically in between the ones obtained with NL1 and NLSH, so for simplicity they are not shown.

^{62}Zn . The comparison of calculated and “experimental” effective alignments in the pairs $^{58}\text{Cu}/^{60}\text{Zn}$ and $^{60}\text{Zn}/^{62}\text{Zn}$ [see Fig. 3(b)] indicates that the configurations $[21,21]^-$ and $[22,24]^+$ are most likely candidates for the bands observed in ^{58}Cu and ^{62}Zn , respectively. The configuration $[21,21]^-$ in ^{58}Cu is calculated to be energetically favored over a considerable spin range in both approaches and also in the cranked Hartree-Fock approach with Skyrme forces [8]. The $[22,24]^+$ configuration will be discussed below. With these

configuration assignments, the lowest transition in the highly deformed band of ^{58}Cu with the transition energy of 830 keV corresponds to a spin change of $11^+ \rightarrow 9^+$ and the lowest transition in the SD band of ^{62}Zn with the transition energy of 1993 keV corresponds to a spin change of $20^+ \rightarrow 18^+$. Thus the bands in ^{58}Cu and ^{62}Zn are observed up to 23^+ and 30^+ , respectively. The corresponding experimental values of $J^{(2)}$ and $J^{(1)}$ (under these spin assignments) and, in addition, the experimental effective alignment in the

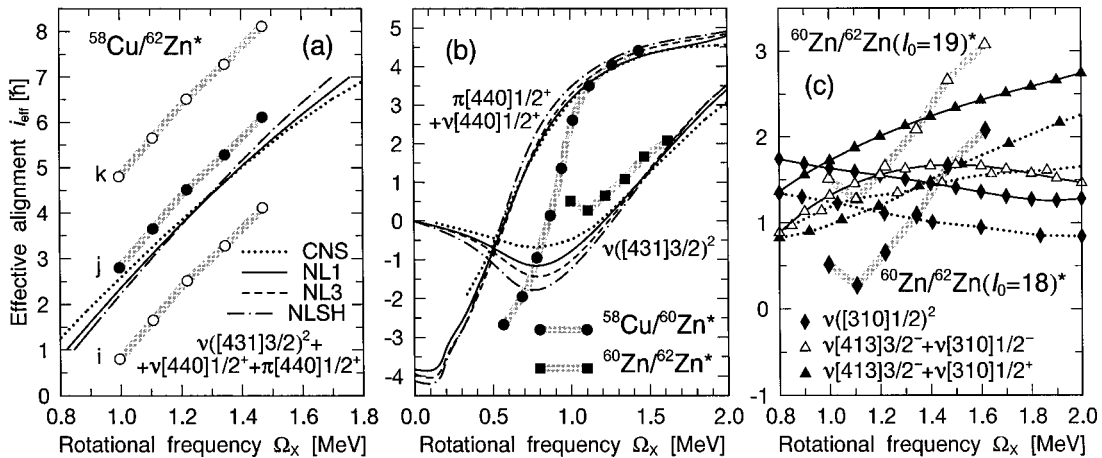


FIG. 3. Experimental and calculated effective alignments. Large symbols on shaded background are used for the experimental values while different types of lines [with symbols in panel (c)] are used for the values calculated in the different models. The compared calculated configurations differ in the occupation of the orbitals shown in the panels. The experimental effective alignment between bands A and B is indicated as A/B. The experimental i_{eff} values are shown at the transition energies of the band indicated by an asterisk (*). In panel (a), the “experimental” i_{eff} values are drawn assuming a fixed spin value of $I_0=9$ for the lowest observed state in the ^{58}Cu band and different spin values $I_0=16$ (i), $I_0=18$ (j), and $I_0=20$ (k) for the lowest state in the ^{62}Zn band. In panels (a) and (b), solid symbols are used for the values of i_{eff} which result from our preferred spin assignments for the bands in ^{58}Cu and ^{62}Zn . Open symbols in panel (a) show that the agreement becomes much worse for other spin assignments consistent with the signatures of the $[21,21]^-$ ^{58}Cu and $[22,24]^+$ ^{62}Zn configurations; see text for details. In panels (b) and (c), the configuration $[22,22]^+$ is used for the SD band in ^{60}Zn . The comparison in panel (c) shows that no reasonable agreement is obtained for the $[22,22]^+$ and $[22,23]^\pm$ ^{62}Zn configurations which were considered in Ref. [1]. In this panel the same type of symbols (open or solid) are used for experimental and theoretical values of i_{eff} which should be compared to be consistent with the signature of the different bands.

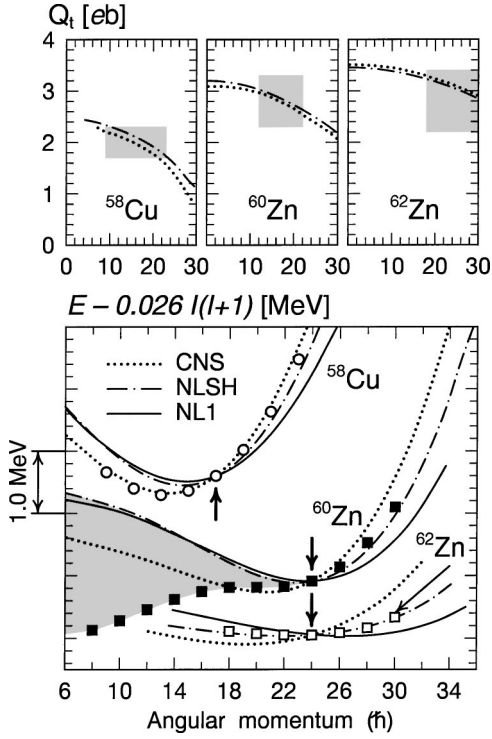


FIG. 4. Bottom panel: calculated (lines) and experimental (symbols) bands shown relative to a rigid rotor reference. The energies of calculated states indicated by arrows are normalized to the corresponding experimental states. The shaded area is used to indicate the possible size of pairing correlations at low spin in the SD band of ^{60}Zn . The results with NL3 are rather close to the ones with NLSH; so for simplicity they are not shown. Top panels: measured transition quadrupole moments Q_t (shaded boxes indicate the upper and lower limits of Q_t and the spin range where they have been measured) versus calculated ones. Since the Q_t values calculated with NL1 and NL3 differ from the ones with NLSH only by $\approx 2-3\%$, only the results of calculations with NLSH are shown.

$^{58}\text{Cu}/^{62}\text{Zn}$ pair are reproduced rather well in the calculations [see Figs. 2 and 3(a)].

The experimental $J^{(1)}$ and $J^{(2)}$ moments of inertia of the ^{62}Zn band are somewhat better described in CRMF theory than in the CNS approach [see Figs. 2(e) and (f)]. The fact that the last experimental point in $J^{(2)}$ is overestimated in the CRMF calculations is possibly due to an interaction between the occupied $[431]3/2^+$ and unoccupied $[431]1/2^+$ orbitals (see bottom panel of Fig. 1). One should note, however, that the configuration $[22,24]^+$ in ^{62}Zn is not calculated as the lowest SD configuration. In the spin range of interest, its energy above the lowest SD solution is $\approx 1-1.5$ MeV in CRMF theory (see, for example, Ref. [20]) and $\approx 0.5-1.0$ MeV in the CNS approach. In Ref. [1], the ^{62}Zn configurations $[22,22]^+$ and $[22,23]^{\pm}$, which are calculated lowest in energy, were considered instead (see also Refs. [20,21]). However, especially when compared with the band in ^{60}Zn , it becomes evident that the experimental values of i_{eff} cannot be reproduced for these configuration assignments [see Fig. 3(c)]. The configuration with only one neutron hole in the $f_{7/2}$ orbital can be excluded for similar reasons but also because its signature partner is calculated degenerate in energy contrary to experiment where no signature partner band has been observed so far.

The calculated high energy of the configuration assigned to the observed band in ^{62}Zn suggests that the parametrizations used might not be optimal with respect of description of single-particle energies in the vicinity of the SD shell gaps. Note, however, that the CNS approach and CRMF theory with three different forces indicate the same group of orbitals in the vicinity of the $N=Z=30$ SD shell gap (see top panel of Fig. 1). In both approaches, the $N=Z=30$ SD shell gap is primarily defined by the energy splitting between the $[440]1/2$ and $[431]3/2$ orbitals originating from the intruder $g_{9/2}$ subshell. Thus the lowering of the $g_{9/2}$ subshell by $\sim 0.5-1$ MeV will almost not affect the size of the $N=Z=30$ SD shell gap but will bring the configuration $[22,24]^+$ in ^{62}Zn closer to the yrast line. Note that this will also make the $N=38$ shell gap seen in Fig. 1 smaller due to the lowering of the $[422]5/2$ orbital. The observation of other SD structures in ^{62}Zn and neighboring nuclei will be essential to establish the ordering of single-particle levels around the $N=30$ SD shell gap and to determine the accuracy with which existing theories describe the alignment properties of single-particle orbitals. This should help to clarify how the models should be further improved to give an even better description of the variety of rotational structures observed in this mass region.

Considering the distribution of particles and holes over high- and low- j orbitals at low spin one obtains the “maximum” spins of the configurations of the observed bands as $I=29^+$ (^{58}Cu), $I=36^+$ (^{60}Zn), and $I=40^+$ (^{62}Zn). Thus the bands in ^{58}Cu and ^{60}Zn (^{62}Zn) are three (five) transitions away from the “maximum” spin. However, the states of “maximum” spin are calculated triaxial both in the CRMF and in the CNS approaches. This behavior can be understood as caused by the interaction between the low- j and high- j orbitals in the $N=3$ shell and is contrary to the shape evolution of bands which terminate in a noncollective prolate ($\gamma=+60^\circ$) or oblate ($\gamma=-120^\circ$) terminating state for $I=I_{\text{max}}$. Even so, the properties of these bands are strongly influenced by the limited angular momentum content of their single-particle configurations. Indeed, several features of these bands are similar to those of smooth terminating bands observed in the $A\sim 110$ mass region [12] and in $^{62,64}\text{Zn}$ [2,22]. Such features are the smooth drop of the dynamic moment of inertia $J^{(2)}$ with increasing rotational frequency to values much lower than the kinematic moment of inertia $J^{(1)}$. Furthermore, a gradual drop of collectivity (i.e., a drop of transition quadrupole moment Q_t) is predicted with increasing spin for both kinds of bands, something which at present has been experimentally confirmed [2,23] only for smooth terminating bands. Indeed, in the $A\sim 60$ region, one can see the gradual transition from the smooth terminating bands in $^{62,64}\text{Zn}$ over the highly deformed band in ^{58}Cu to the SD bands in $^{60,62}\text{Zn}$. Calculations for a number of configurations in neighboring nuclei and in ^{68}Zn (see Ref. [24] for this nucleus) show that the above-mentioned features are common for the SD and highly deformed bands in the $A\sim 60-70$ mass region. Thus a rigid-rotor assumption ($J^{(1)}\approx J^{(2)}$) sometimes used in the analysis of SD bands is not valid in this mass region. Indeed, in line with previous studies [25], we can conclude that it is not so much the deformation (at $I=0$) of a band which determines if it is rigid-rotor-like or not but rather how far away the band is from its

“maximum” spin value. Therefore, it is in general much more difficult to find rigid-rotor-like rotational bands in light nuclei because the “maximum” spin within the yrast and near-yrast configurations is generally much lower than in heavier nuclei. For example, large differences between $J^{(1)}$ and $J^{(2)}$ are not expected in the SD bands in the $A \sim 150$ mass region because the “maximum” spin of their configurations, $I_{\max} \sim (150-200)\hbar$, is far above the experimentally accessible spin values (see Ref. [25]). Thus, the experimental study of SD bands in the $A \sim 60$ region up to their “maximum” spin values would be very important for general understanding of the very-high-spin properties of SD bands.

One should note the important role of the first two $f_{7/2}$ holes (in $[303]7/2$ orbitals at prolate shape) in the stabilization of high deformation and superdeformation for nuclei around $Z=N=30$. Their influence is twofold. First, they significantly contribute to the quadrupole moment (see Ref. [26]). In this respect the highly deformed and SD bands in the $A \sim 60$ mass region are similar to the ones in the $A \sim 135$ mass region, where the proton $g_{9/2}$ holes play an important role in stabilization of superdeformation (see Ref. [27]). Second, the contribution to the “maximum” spin of these $f_{7/2}$ holes is comparable with the contribution from $g_{9/2}$ particles. For example, full alignment of two highest $f_{7/2}$ holes gives $6\hbar$, while full alignment of two lowest $g_{9/2}$ particles gives $8\hbar$ in angular momentum.

The SD and highly deformed bands in the $A \sim 60$ mass region are characterized by very large transition energies reaching 3.2 MeV or more at the top of all three bands studied here. For these bands, the excitation energies drawn relative to the rigid-rotor reference appear to provide the best measure of how well the theory describes the response of nuclei to the rotation as illustrated in the bottom panel of Fig. 4. Note, however, that since pairing correlations are neglected in the calculations, the comparison between theory and experiment should be made not with respect to the ground state, but with respect to some high-spin state. Indeed, in this kind of plot the difference between different approaches and different parametrizations of the RMF theory is more clearly seen compared with the plot of dynamic and kinematic moments of inertia (see Fig. 2). Comparing different results one can conclude that the best description of ex-

citation energies within bands at high spin is obtained within the CRMF theory with the NLSH and NL3 forces for $^{60,62}\text{Zn}$ while the band in ^{58}Cu is somewhat better described in the CNS approach. Concerning relative energies of different configurations (not shown in Fig. 4), none of the approaches give the configuration assigned to the SD band in ^{62}Zn as yrast with somewhat larger discrepancies in the CRMF than in the CNS approach.

IV. CONCLUSIONS

In conclusion, the cranked relativistic mean field theory and the configuration-dependent cranked Nilsson-Strutinsky approach have been used for a study of superdeformed and highly deformed rotational bands in the $A \sim 60$ mass region. Experimental observables like the dynamic moment of inertia $J^{(2)}$ and the transition quadrupole moments Q_i are well described in both approaches. It was found that a much lower value of the dynamic $J^{(2)}$ than the kinematic $J^{(1)}$ moment of inertia at high spin is rather a general feature of SD and highly deformed bands in this mass region, reflecting the limited angular momentum content in these configurations. Using the fact that the yrast SD band in ^{60}Zn is linked to the low-spin level scheme it was shown that by means of the effective alignment approach, it is possible to establish absolute spin values for the unlinked highly deformed and superdeformed bands in neighboring nuclei. Thus for the first time it becomes possible to compare theory with experiment in a direct way also for spin-dependent physical observables like the kinematic moment of inertia, $J^{(1)}$, and excitation energies as a function of spin, $E(I)$, for superdeformed bands in the unpaired regime. It appears likely that it should be possible to link the bands in ^{58}Cu and ^{62}Zn to the low-spin level scheme in the near future and thus to test the present assignments experimentally.

ACKNOWLEDGMENTS

A.V.A. acknowledges support from the Alexander von Humboldt Foundation. This work was also supported in part by the Bundesministerium für Bildung und Forschung under Project No. 06 TM 875 and by the Swedish Natural Science Research Council.

-
- [1] C.E. Svensson, C. Baktash, J.A. Cameron, M. Devlin, J. Eberth, S. Flibotte, D.S. Haslip, D.R. LaFosse, I.Y. Lee, A.O. Macchiavelli, R.W. MacLeod, J.M. Nieminen, S. D. Paul, L.L. Riedinger, D. Rudolph, D.G. Sarantites, H.G. Thomas, J.C. Waddington, W. Weintraub, J.N. Wilson, A.V. Afanasjev, and I. Ragnarsson, *Phys. Rev. Lett.* **79**, 1233 (1997).
- [2] C.E. Svensson, C. Baktash, G.C. Ball, J.A. Cameron, M. Devlin, J. Eberth, S. Flibotte, A. Galindo-Uribarri, D.S. Haslip, V.P. Janzen, D.R. LaFosse, I.Y. Lee, A.O. Macchiavelli, R.W. MacLeod, J.M. Nieminen, S.D. Paul, D.C. Radford, L.L. Riedinger, D. Rudolph, D.G. Sarantites, H.G. Thomas, J.C. Waddington, D. Ward, W. Weintraub, J.N. Wilson, A.V. Afanasjev, and I. Ragnarsson, *Phys. Rev. Lett.* **80**, 2558 (1998).
- [3] I. Ragnarsson, in *Proceedings of the Workshop on the Sci-*

ence of Intense Radioactive Ion Beams, edited by J. B. McClelland and D. J. Vieira, Los Alamos National Laboratory Report No. LA-11964-C, 1990, p. 199.

- [4] C.E. Svensson, D. Rudolph, C. Baktash, M.A. Bentley, J.A. Cameron, M.P. Carpenter, M. Devlin, J. Eberth, S. Flibotte, A. Galindo-Uribarri, G. Hackman, D.S. Haslip, R.V.F. Janssens, D.R. LaFosse, T.J. Lampman, I.Y. Lee, F. Lerma, A.O. Macchiavelli, J.M. Nieminen, S.D. Paul, D.C. Radford, P. Reiter, L.L. Riedinger, D.G. Sarantites, B. Schaly, D. Seweryniak, O. Thelen, H.G. Thomas, J.C. Waddington, D. Ward, W. Weintraub, J.N. Wilson, C.H. Yu, A.V. Afanasjev, and I. Ragnarsson, *Phys. Rev. Lett.* **82**, 3400 (1999).
- [5] I. Ragnarsson, *Phys. Lett. B* **264**, 5 (1991).
- [6] I. Ragnarsson, *Nucl. Phys.* **A557**, 167c (1993).

- [7] A.V. Afanasjev, G. Lalazissis, and P. Ring, Nucl. Phys. **A634**, 395 (1998).
- [8] D. Rudolph, C. Baktash, J. Dobaczewski, W. Nazarewicz, W. Satuła, M.J. Brinkman, M. Devlin, H.-Q. Jin, D.R. LaFosse, L.L. Riedinger, D.G. Sarantites, and C.-H. Yu, Phys. Rev. Lett. **80**, 3018 (1998).
- [9] W. Koepf and P. Ring, Nucl. Phys. **A493**, 61 (1989).
- [10] W. Koepf and P. Ring, Nucl. Phys. **A511**, 279 (1990).
- [11] T. Bengtsson and I. Ragnarsson, Nucl. Phys. **A436**, 14 (1985).
- [12] A.V. Afanasjev and I. Ragnarsson, Nucl. Phys. **A591**, 387 (1995).
- [13] L.B. Karlsson, I. Ragnarsson, and S. Åberg, Nucl. Phys. **A639**, 654 (1998).
- [14] J. Dudek, W. Nazarewicz, and P. Olanders, Nucl. Phys. **A420**, 285 (1984).
- [15] A.V. Afanasjev, J. König, and P. Ring, Nucl. Phys. **A608**, 107 (1996).
- [16] P.-G. Reinhard, M. Rufa, J. Maruhn, W. Greiner, and J. Friedrich, Z. Phys. A **323**, 13 (1986).
- [17] G.A. Lalazissis, J. König, and P. Ring, Phys. Rev. C **55**, 540 (1997).
- [18] M.M. Sharma, M.A. Nagarajan, and P. Ring, Phys. Lett. B **312**, 377 (1993).
- [19] J. König and P. Ring, Phys. Rev. Lett. **71**, 3079 (1993).
- [20] H. Madokoro and M. Matsuzaki, nucl-th/9803058.
- [21] D. Rudolph, C. Baktash, W. Satuła, J. Dobaczewski, W. Nazarewicz, M.J. Brinkman, M. Devlin, H.-Q. Jin, D.R. LaFosse, L.L. Riedinger, D.G. Sarantites, and C.-H. Yu, Nucl. Phys. **A630**, 417c (1998).
- [22] A. Galindo-Uribarri, D. Ward, G.C. Ball, V.P. Janzen, D.C. Radford, I. Ragnarsson, and D. Headly, Phys. Lett. B **422**, 45 (1998).
- [23] R. Wadsworth, R.M. Clark, J.A. Cameron, D.B. Fossan, I.M. Hibbert, V.P. Janzen, R. Krücken, G.J. Lane, I.Y. Lee, A.O. Macchiavelli, C.M. Parry, J.M. Sears, J.F. Smith, A.V. Afanasjev, and I. Ragnarsson, Phys. Rev. Lett. **80**, 1174 (1998).
- [24] M. Devlin, A.V. Afanasjev, R.M. Clark, D.R. LaFosse, I.Y. Lee, F. Lerma, A.O. Macchiavelli, R.W. MacLeod, I. Ragnarsson, P. Ring, D. Rudolph, D.G. Sarantites, and P.G. Thirolf, Phys. Rev. Lett. (submitted).
- [25] I. Ragnarsson, Phys. Lett. B **199**, 317 (1987).
- [26] J. Dobaczewski, nucl-th/9801056.
- [27] A.V. Afanasjev and I. Ragnarsson, Nucl. Phys. **A608**, 176 (1996).